Implications of Mitigating the Ozone and Fine Particulate Matter Pollution in the Greater Bay Area Using a Regional-to-Local Coupling Model

Xuguo Zhang[1,2], Jenny Stocker[3], Kate Johnson[3], Yik Him Fung[2], Teng Yao[2], Christina Hood[3], David Carruthers[3], and Jimmy C. H. Fung[1,2,*]

[1] Department of Mathematics, The Hong Kong University of Science and Technology, Hong Kong.

[2] Division of Environment and Sustainability, The Hong Kong University of Science and Technology, Hong Kong.

[3] Cambridge Environmental Research Consultants, Cambridge, UK.

Corresponding author: Jimmy C. H. Fung (majfung@ust.hk)

Key Points:

- A novel regional-to-local coupled model was set up to explore the likely impact of emissions reductions and pollution mitigation pathways.
- Substantial NO_x controls in the traffic sector worsened the urban O_3 concentration, revealing the VOC-limited formation regime.
- Probing into frequent summer O_3 episodes emphasized the value of more stringent VOC controls, in particular for the industrial sector.

ORCID: 0000-0001-7857-2525 (X. Zhang); 0000-0003-3243-7226 (J. Stocker); 0000-0002-7071-1137 (Y.H. Fung); 0000-0001-9244-5696 (C. Hood); 0000-0002-7859-8511 (J.C.H. Fung)

Abstract

Ultrahigh-resolution air quality models resolving sharp concentration gradients benefit health calculations. Mitigating fine particular matter ($PM_{2.5}$) in the past decade triggered ozone (O_3) deterioration in China. Effectively controlling both pollutants is still understudied from an ultrahigh-resolution perspective. This study proposes a coupled regional-to-local-scale modeling system suitable for quantitatively mitigating pollution pathways at various resolutions. Sensitivity scenarios for controlling nitrogen oxide (NO_x) and volatile organic compounds (VOC) emissions, concentrating on traffic and industry sectors, are explored. The results show that concurrent controls on both sectors lead to an overall 17%, 5%, and 47% emission reduction in NO_x, $PM_{2.5,}$ and VOC, respectively. The 50% less traffic scenario leads to reduced NO_2 and $PM_{2.5,}$ but increased O_3 concentrations in urban areas, revealing a VOC-limited regime. The reduced industrial VOC emission scenario leads to reduced O_3 concentrations throughout the mitigation domain. The maximum decrease in the median of hourly NO_2 is over 11 µg/m³, while the maximum increase in the median of maximum 8-hour rolling O_3 is over 10 µg/m³ for the reduced traffic scenario. When both the traffic and industrial controls are applied, the impact on O_3 reduces to an increase of less than 7 µg/m³. The daily-averaged $PM_{2.5}$ decreases by less than 2 µg/m³ for the reduced traffic scenario and varies little for the reduced VOC scenario. An O_3 episode analysis for both controls scenarios leads to O_3 decreases of up to 15 µg/m³ (8-h metric) and 25 µg/m³ (1-h metric) in a rural area to the northeast of the mitigation domain.

Plain Language Summary

Spatial concentration maps of air pollutants showing variations over small distances are useful for assessing human health in metropolitan regions. The combined control of fine particulate matter and ozone has not yet been fully understood at high resolution. This study implements a regional-to-local urban modeling system for quantitatively assessing possibilities for pollution reduction. Typical air pollutants are explored, concentrating on emissions from traffic and industry source sectors. We find that combined control on both sectors leads to considerable emission reductions. The scenario analysis reveals the most substantial factors affecting ozone pollution in various locations. The contributions of air pollution from both sectors are assessed. The research findings would improve the awareness of air quality management strategies and benefit multi-level governments for joint control of regional air pollution problems.

Index Terms

3355 Regional modeling (4316); 0345 Pollution: urban and regional (0305, 0478, 4251, 4325); 0545 Modeling (1952, 4255, 4316); 3329 Mesoscale meteorology; 6620 Science policy (0485, 4338).

Keywords

street-scale; air dispersion model; CMAQ-ADMS-Urban; sensitivity analysis; ozone; Greater Bay Area.

1 Introduction

Air pollution has generated significant interest in recent years due to its adverse effects on human health (Che et al., 2020; Conibear et al., 2021; Wu et al., 2019) and mitigation of climate change (Li et al., 2019c; Qin et al., 2017). It has become an urgent and intractable issue since Chinese president Xi announced a bold pledge that Chinese carbon emissions would peak before 2030 and China would become carbon neutral by 2060 (Cheng et al., 2021; Cui et al., 2021). The Chinese government has devoted tremendous efforts and released a series of emissions control policies to address this challenge (Cai et al., 2018; Jiang et al., 2015; Wu et al., 2019; Zhang et al., 2020). Zhang et al. (2020) revealed a holistic emissions control picture by utilizing a chemical transport model method to assess the implemented emissions control policies covering various sectors during the 13th Five-Year-Plan in China. In response to the stringent national controls, ambient fine particulate matter ($PM_{2.5}$) has decreased substantially while ozone (O_3) pollution levels are becoming severe (Li et al., 2019b; Zhao et al., 2021). The combined health effect has been improved during the past decade (Zhang et al., 2021a), although high O_3 concentrations have an adverse effect on habitats (Yli-Pelkonen et al., 2017), so they must, in the long-term, also be controlled. Strategies for effectively controlling the absolute concentrations of O_3 and $PM_{2.5}$ simultaneously in urban regions, where people spend the majority of their time, are of increasing interest and importance.

A growing number of studies have devoted great efforts to the mechanism of coupled O_3 and $PM_{2.5}$ pollution levels in various regions in China. Li et al. (2019a) firstly found the major reason for worsening O_3 was due to the significantly reduced $PM_{2.5}$ that led to fewer hydroperoxy radicals for O_3 formation since 2013 in the North China Plain (NCP). Zhao et al. (2021) confirmed the interactions between the two pollutants and called for the concurrent control of both pollutants following analysis of four-year observational data in China. Li et al. (2019b) proposed to reduce the nitrogen oxide (NO_x) and volatile organic compound (VOC) emissions aggressively to control both pollutants in the NCP by analyzing summer O_3 surface data from 2013-2018. Gong et al. (2021) utilized the Community Multiscale Air Quality (CMAQ) model at 12 km resolution to trace the precursors of $PM_{2.5}$ and O_3; the cross-boundary transport effect on the two-pollutant interaction was found in the Yangtze River Delta (YRD). In addition, Li et al. (2021a) concluded that the industrial and traffic emission source sectors dominated contributions to both pollutants in YRD, also through CMAQ at 12 km resolution. Thus recent literature motivates studies on the impact of NO_x and VOC emissions from traffic and industry in China.

Other studies have focused efforts on quantifying the effect of model resolutions on air pollution simulations and health calculations. A previous study in the US proved that finer resolution (comparing 4 km and 12 km grid spacing) of a CMAQ model was better for calculating health effects in urban areas; the results were comparable in rural areas (Jiang and Yoo, 2018). Tao et al. (2020) found that the finer-resolution modeling could better capture and reproduce the temporal trends and magnitudes of meteorological conditions and air quality in Beijing. On the contrary, a local study indicated that grid resolution has little effect on the simulation of $PM_{2.5}$ and O_3 in YRD (Wang et al., 2021). Liu et al. (2020) demonstrated that model resolution did not significantly improve predictions for $PM_{2.5}$ and daily maximum 8-hour O_3 in Nanjing. However, the spatial distributions of both pollutants were better captured with a finer resolution model, leading to in excess of 20% difference in premature mortality due to exposure to O_3. The impact of model resolutions on pollutant simulations and health calculations varied in different cities or regions (urban or rural) within an agglomeration. Consequently, it is of great interest to explore whether higher resolution modeling techniques benefit model simulations for highly urbanized cities.

Previous studies have, for the most part, used a coarse resolution (>1 km) model and an observations-oriented method to explore pollution sources or calculate health effects for the coupled two-pollutant system (Li et al., 2021b; Silver et al., 2020). Although a previous study (Silveira et al., 2019) summarized a great number of coupled regional-to-local models which have been applied in worldwide urban regions, the model calculation algorithms and assumptions varied widely between studies. The presented regional-to-local scale coupling system follows the approach introduced in (Hood et al., 2018; Stocker et al., 2012). In this system, double-counting of local emissions is avoided by deducting local modelling of all emissions represented as grid sources from the regional modelling of all emissions before adding street-scale local modelling with explicit and gridded sources. The local modelling of road sources in ADMS-Urban can include street canyon effects, which affect the predicted concentrations both inside and outside the canyon (Hood et al., 2021). The ADMS-Urban street canyon module was designed to account for street canyons with higher H/W ratios than the popular Operational Street Pollution Model (OSPM) model, which was developed for H/W ratio around 1. Very few studies have applied coupled regional and very high-resolution (street-level) modeling techniques to investigate the traffic and industrial contribution to the complex coupled two-pollutant problem through emission scenario testing. A street-scale model that provides a detailed representation of the spatial variation of pollutant gradients has clear advantages in terms of calculating health exposure, compared with previous studies applying regional or global models.

Although urban-scale models have investigated air pollution interactions in megacities, very few coupled model systems were applied based on an Urban Atmospheric Dispersion Modelling System (ADMS-Urban) and CMAQ model for the metropolitan region of the Greater Bay Area (GBA). Zhang et al. (2015) integrated CMAQ and the CALifornia PUFF (CALPUFF) model to simulate the contribution of SO_2 concentration due to local emissions in GBA region. A regional European Monitoring and Evaluation Program Unified Model for the UK (EMEP4UK) was coupled with ADMS-Urban to perform street-level air pollutant simulations in London (Hood et al., 2018). Although ADMS-Urban was applied within the sixth-ring in Beijing for simulating various pollutants (Biggart et al., 2020), the background concentration level was adapted directly from measurement data and was assumed uniformly distributed across the model domain, instead of coupling with a regional model. As a result, the current study is the first localized coupled regional-to-local scale model system consisting of ADMS-Urban and CMAQ to assess the sensitivity of two pollutants to emissions from traffic and industrial sectors in the GBA. The motivation for targeting the two sectors relates to the importance of the O_3 precursors, VOC and NO_x, from the anthropogenic industrial and traffic sectors in GBA, respectively. Consequently, assessing the impact of changes to emitted NO_x (and hence NO_2) and VOCs is of interest. Section 2 of this article describes the regional and local street-scale model configuration and the sensitivity scenarios. Regional and local model simulation results and the model performance of selected monitoring stations are discussed in section 3. Section 4 presents a discussion of research findings, followed by conclusions in section 5.

2 Research Methods

2.1 Model configuration

The street-scale resolution ADMS-Urban dispersion model has been coupled with the CMAQ regional model configuration to investigate O_3 and $PM_{2.5}$ concentrations and the sensitivity of both pollutants to emissions from the traffic and industrial sectors. The regional CMAQ model has been widely used in assessing holistic emission control policies (Zhang et al., 2020), combined health effects (Zhang et al., 2021a), and data assimilation of model bias corrections (Zhang et al., 2021b) in our previous publications. In terms of the regional model configuration, the detailed setting is given in the aforementioned publications, and only key points have been listed below. The Sparse Matrix Operations Kernels Emissions (SMOKE) model has been used to process the localized bottom-up emission inventory, including industrial sources, mobile sources, power plants, residential sources, and marine sources for the GBA. The marine emissions have been split into Ocean Going Vessels (OGV), Local Vessels (LV), and River Vessels (RV) and were calculated using Automatic Identification System (AIS) data. The emission inventory for outside GBA has been adapted from the Multi-resolution Emission (MEIC) data (Tong et al., 2020). As shown in Figure S1, four nested domains with resolutions of 27 km (D1), 9 km (D2), 3 km (D3), and 1 km (D4) were utilized for the regional CMAQ model. The boundary conditions of the outermost D1 domain were obtained from a global chemical transport model (GEOS-chem) (Lam and Fu, 2010); boundary conditions for the nested domains D2-D4 were obtained from the respective mother domains. Outputs from the SMOKE and CMAQ models were used to drive the ADMS-Urban model.

ADMS-Urban is a street-scale resolution, quasi-Gaussian plume dispersion model from the Atmospheric Dispersion Modeling System (ADMS) family, which has already been widely applied across the world to assess the environmental impact, control policies, and pollution concentration forecasts (Biggart et al., 2020; Carruthers et al., 1994; Hood et al., 2018; Lao and Teixidó, 2011). The model simulates the dispersion of pollutant emissions in urban areas by: representing sources at high spatial resolution (primarily traffic and industry); modeling the influence of urban morphology on dispersion processes (street canyons, building density, tunnels, road elevation); and applying simplified, near-field chemical schemes. Sharp concentration gradients resulting from emissions released from sources such as traffic can be resolved in the model calculations and captured for output using the irregularly-spaced receptor grid generated by the model. Spatially varying meteorological parameters from the Weather Research and Forecast (WRF) model, such as wind and surface sensible heat flux, have been used as input into the ADMS-Urban model to drive pollutant dispersion (Hood et al., 2018). ‘Background’ pollutant concentrations, representing long-range pollutant transport, have been derived from the hourly simulation data of the CMAQ model. Due to a lack of representative source parameters (stack heights, efflux parameters), industrial and power plant sources have been coarsely represented in the regional model using appropriate factors to disaggregate emissions vertically, while an explicit road network was applied to distribute the ground-level traffic emissions within the ADMS-Urban model. Different weighting factors were given to different types of roads, but the same factors were assigned to different species. The road network data were obtained from the OpenStreetMap source (http://openstreetmap.org/), with some minor roads removed to reduce the computational expense.   A more detailed description of the coupling methodology between a regional model and ADMS-Urban can be found in our previous publication (Hood et al., 2018).

2.2 Sensitivity scenario design

The control measures affecting emissions from traffic and industrial sectors are applied in the regional CMAQ model over the Pearl River Delta Economic Zone (PRD EZ), while explicit traffic emissions scenarios are applied to the road traffic network modelled in ADMS-Urban. Four potential sensitivity scenarios are designed. As shown in Table 1, the Base case is a business as usual (BAU) scenario for both the regional CMAQ model and the local ADMS-Urban model. Evaluation of the system is performed for a historical period where measurement data are readily available. Meteorological conditions influence the likelihood of O_3 episodes. Since higher concentrations are recorded in the spring and autumn of 2019, O_3 episodes in April and May 2019 are chosen for the control measures scenario study. In table 1, three control scenarios are listed. Since NO_x and VOC are important precursors for O_3 formation, the non-linear relationship between the precursors and O_3 is of great importance. Due to the short lifetime of NO_x, which is emitted mainly from the traffic sector, the Half-traffic case considers a 50% reduction in traffic emissions for all the standard pollutants in the coupled modeling system. Since the majority of anthropogenic VOC emissions are from the industrial sector, the Half-industry case considers the 50% reduction in industrial VOC emissions only in the regional model but with BAU in the local model. The Both control case integrates the control measures in both the Half-traffic and Half-industry scenarios.

Table 1. Scenario design for the coupling system

Scenarios	**I. Base case**	**II. Half Traffic case**	**III. Half Industry VOC case**	**IV. Both Control case**
Scenario description	Business As Usual (BAU)	50% reduction in traffic emissions	50% reduction in industrial VOC emissions	Scenarios II & III
Regional model emissions	BAU	50% emission reduction in Mobile sector (all pollutants)	50% emission reduction in VOC from Industrial sector	50% emission reduction in a) mobile sector (all pollutants) and b) VOC emissions from the industrial sector
Local model emissions	BAU	50% reduction in emissions from explicitly defined road traffic sources	BAU	50% reduction in emissions from explicitly defined road traffic sources

2.3 Scenario emissions comparison

It is important to put the '50% reduction' control measures in the context of the total emissions. A summary of total annual anthropogenic NO_x, VOC, and $PM_{2.5}$ emissions for the regional model domain covering central GBA is presented in Figure S2. Note that both the 'point' and 'area' emissions categories are considered to represent primarily industrial activities, with VOC emissions affected by the 'half industry' control. Relative to total emissions, the maximum reduction for NO_x is approximately 17% and for $PM_{2.5}$ is only 5%. For VOCs, which are impacted by both control measures, emissions are reduced by a much larger amount, 47%. However, it is important to note that total VOC emissions also have a large contribution from biogenic sources (around 50%), so in real terms, the maximum VOC reduction due to control measures is closer to 25%. In terms of traffic emissions reductions, the scenario modelled corresponds to a reduction in vehicle numbers and/or distances driven, rather than improvements in vehicle technologies. Whilst technological improvements (including the introduction of electric vehicles) can reduce tailpipe emissions to zero, non-exhaust particulate emissions such as brake and tyre wear are a direct result of vehicle activity. Consequently, non-exhaust vehicle emissions are not mitigated by improvements to engine technology, although there may be associated technological improvements in relation to non-exhaust emissions, such as regenerative braking.

Some example emissions plots for the 1 km domain are shown in Figure S3 to Figure S8. All emissions presented are given as 'daily column' values, i.e., the values correspond to daily average emissions summed over all vertical levels included in the modeled 3D emissions grids. In the regional model, VOCs are a complex mixture of different components. For the purpose of the emissions plots shown here, paraffin (PAR) emissions have been used as a species representative of total VOCs. Figure S3 compares the total PAR emissions for the BAU case and the three scenarios. Visually, the reduction in PAR emissions on the roads can be seen by comparing Figures S3a and S3b, i.e., the signature of the road sources is reduced; comparing Figures S3a and S3c highlights the reduction in industrial source emissions; and Figure S3d shows the result of both reductions. Figure S4 presents spatial plots of differences which emphasize the change in emissions. Figure S4a clearly indicates reductions in the road network in the difference between the base case and the reduced traffic scenario. At the same time, Figure S4b shows large reductions at locations where there is intensive industrial activity (Shenzhen, Dongguan, and Guangzhou). Similar patterns of NO_x and $PM_{2.5}$ could be found in Figure S5 and S7, respectively. The reduction in VOC has no effects on NO_x and $PM_{2.5}$ emissions, as shown in Figures S6b and S8b.

3 Results

The regional model has been configured and run for April – May 2019. The coupled system results have been generated for the same period for the urban sub-domains developed as a demonstration area for this study, i.e., a 6 km x 6 km area in central Guangzhou. Period-average concentrations have been calculated. Both urban and rural monitors have been selected to illustrate the pollution variation.

3.1 Regional model period-average air quality maps

Figures 1a and 1b show period-average NO_2 concentrations for major PRD EZ for the base case and the half traffic case respectively, at 1 km grid resolution. As expected, there is a clear reduction in Guangzhou and Shenzhen NO_2 concentrations due to the half traffic emissions scenario. NO_2 concentrations are significantly higher in the HKSAR (to the south of Shenzhen), in industrial areas towards Guangzhou, and also along shipping lanes than in the urban area. Figure 1c quantifies the reduction in NO_2 concentrations for this period; concentrations are reduced by up to 5 ppb in central Guangzhou and Shenzhen.

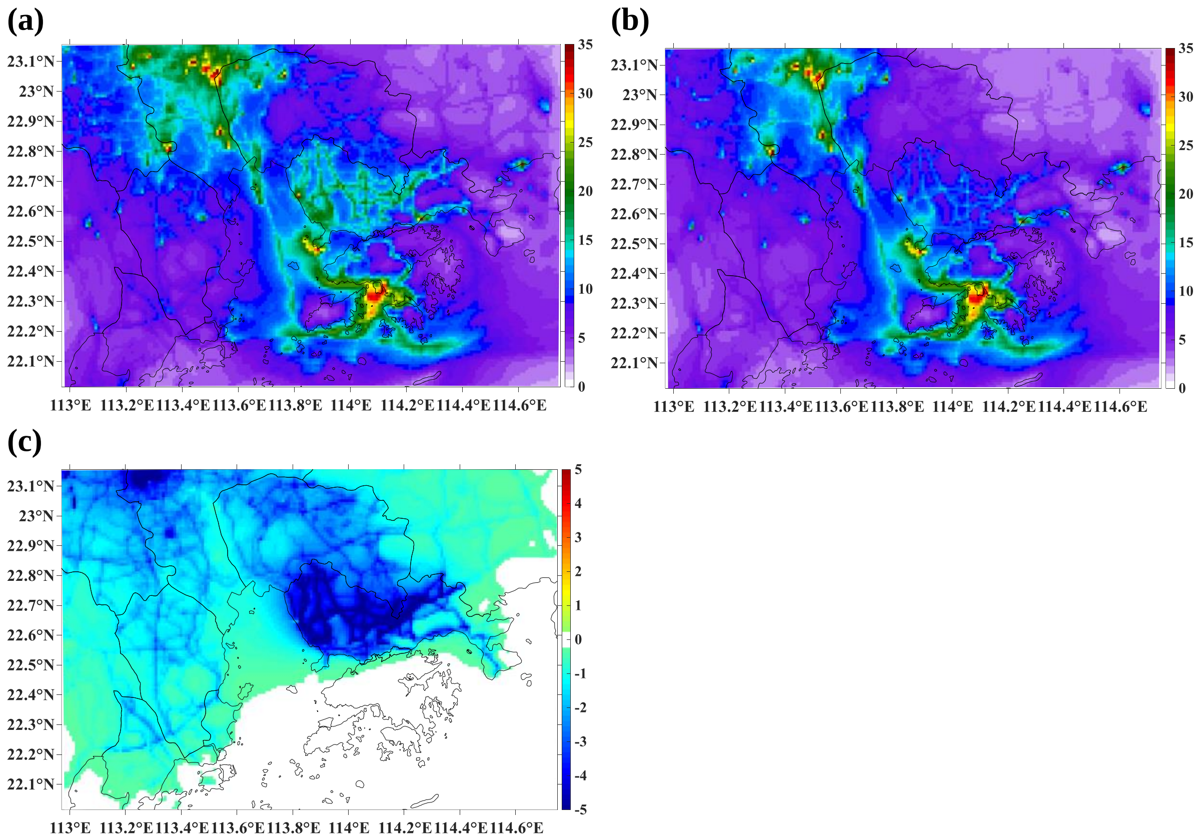

Figure 1. Simulated spatial maps of period-average NO_2 concentrations for (a) Base case, (b) Half Traffic case, and (c) Difference plot: Both controls – Base case (ppb)

Figures 2a and 2b compare period-average O_3 concentrations for major PRD EZ for the base case and both controls together respectively. Due to the reduction in NO_x concentrations leading to a reduction in O_3 titration by NO_x, O_3 concentrations increase in Shenzhen as a result of the emissions controls. Conversely, in the rural areas to the northeast of the domain, downwind of the highly polluting areas, O_3 concentrations decrease due to the controls because, overall, less oxidant (the sum of NO_2 and O_3) is present in the atmosphere.

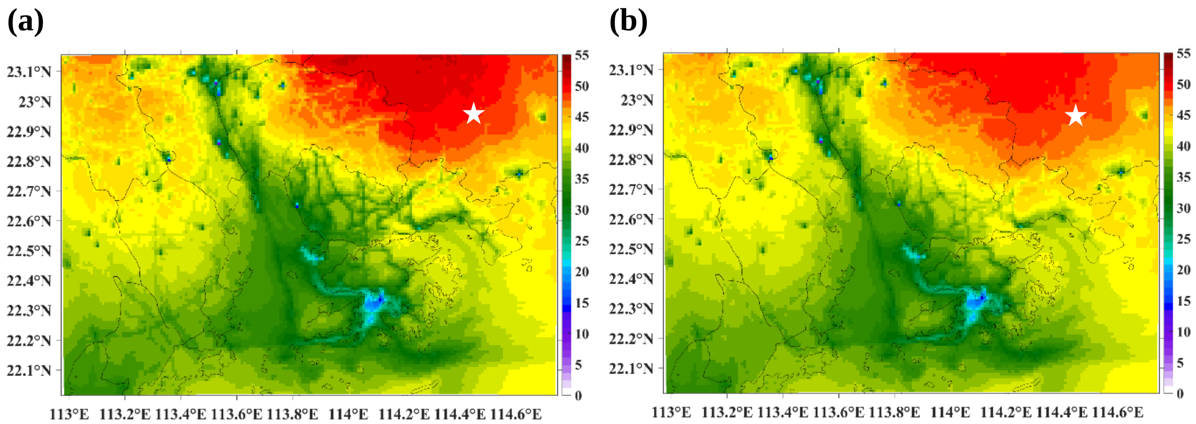

Figure 2. Simulated spatial maps of period-averaged O_3 for (a) Base case and (b) Both controls (ppb); white star indicates the location for further quantification of regional model concentrations (Figure 3)

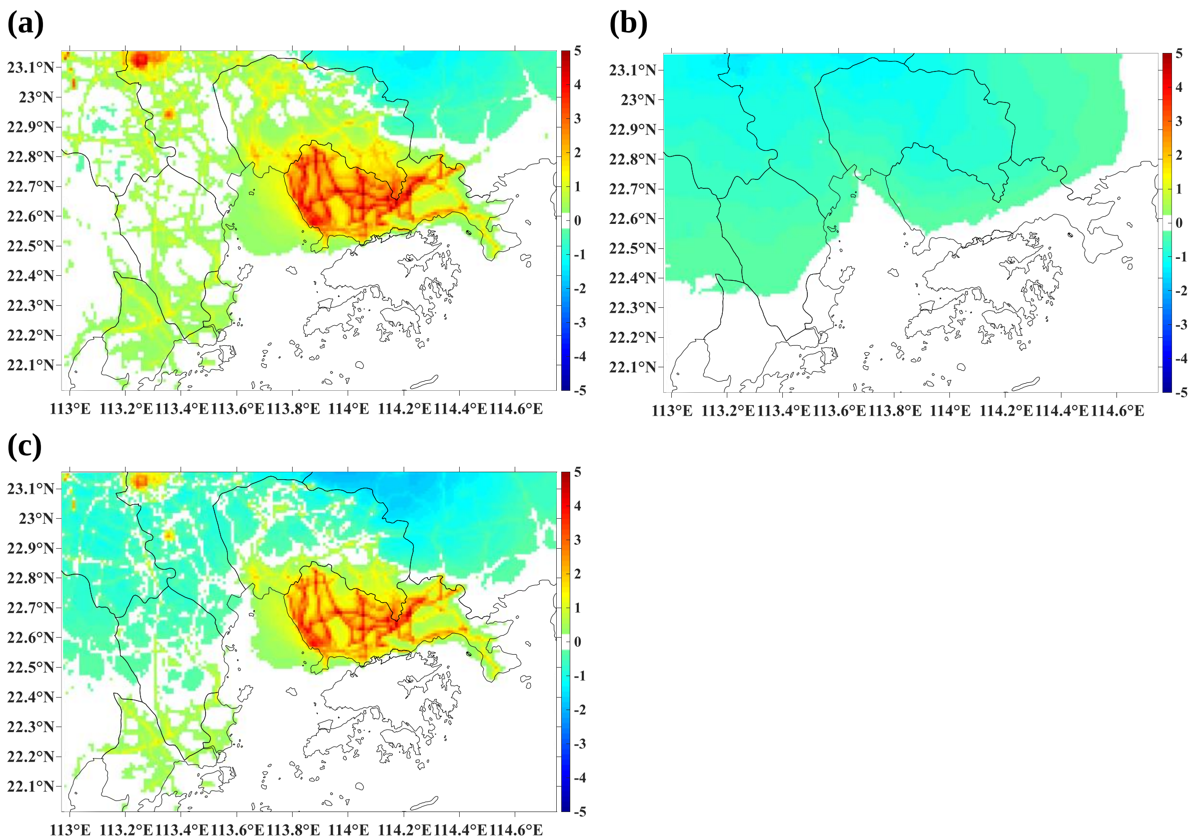

Figure 3. Simulated spatial maps of period-averaged O_3 concentrations - Difference plots for (a) Half Traffic – Base case; (b) Half Industry VOC – Base case, and (c) Both controls – Base case (ppb).

Figures 3a to 3c quantify the changes in O_3 concentrations for this period, for each of the controls and both controls together. Figure 3a relates to the half traffic case;

concentrations increase in the urban areas and decrease downwind in the rural areas due to reduced NO_x titration and lower oxidant emissions, as discussed above. Figure 3b relates to the reduced VOC case; here, O_3 concentrations are reduced throughout the domain because lower concentrations of VOCs correspond to lower levels of reactive species in the atmosphere, resulting in less oxidant (in this case, O_3) being generated. When both controls are considered together, increased O_3 concentrations are still seen in the urban areas. Still, the magnitude is less than in Figure 3a due to the influence of reduced VOC concentrations. In the majority of locations away from the urban areas, O_3 concentrations are reduced, albeit by a relatively small amount (few ppb) when this average O_3 metric is considered.

Figures 4a and 4b show period-average $PM_{2.5}$ concentrations for the PRD EZ for the base case and the half traffic case respectively, at 1 km grid resolution. Although inspection of Figure 4c would suggest that emissions reductions are minimal, in fact, considerable $PM_{2.5}$ concentration differences result from the traffic restrictions imposed in the urban areas. Figure 4c quantifies the reduction in $PM_{2.5}$ concentrations for this period; concentrations are reduced by up to 3 µg/m³ in central Shenzhen.

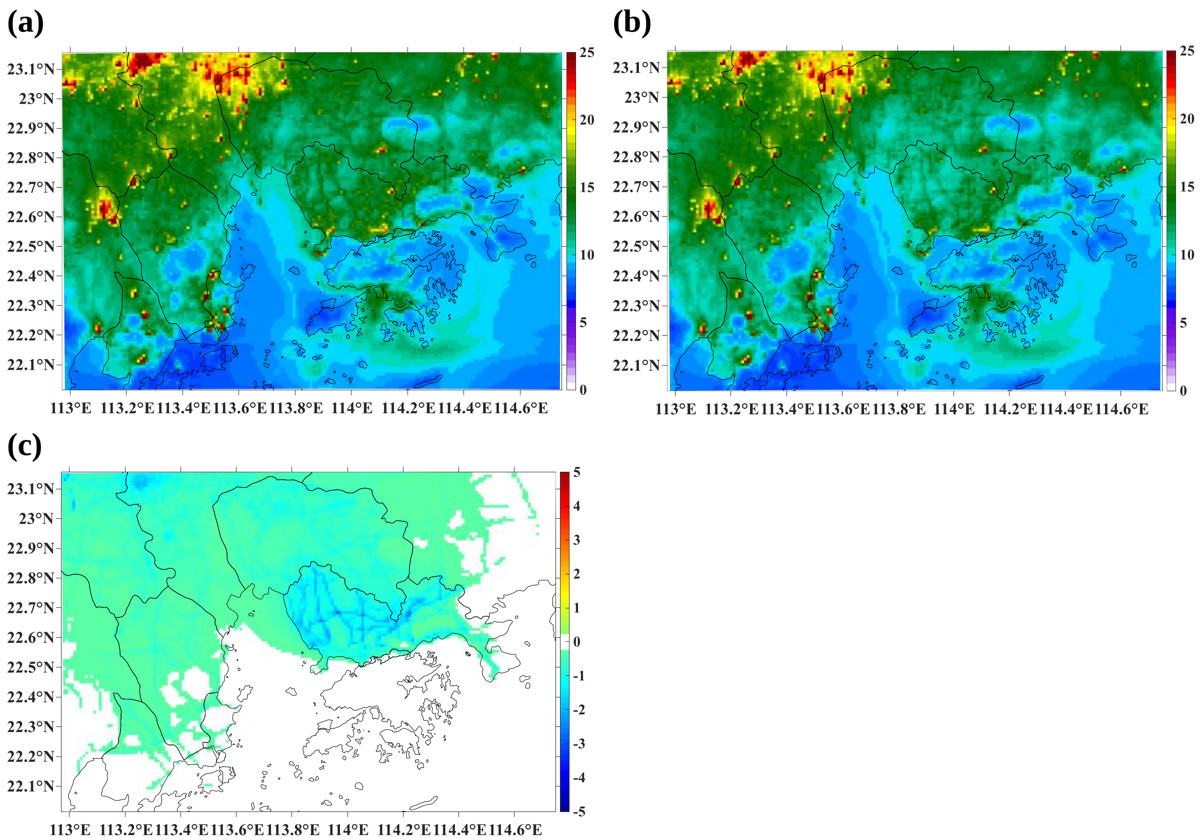

Figure 4. Simulated spatial maps of period-average $PM_{2.5}$ concentrations for (a) Base case, (b) Half Traffic case, and (c) Difference plot: Both controls – Base case (µg/m³).

3.2 Coupled system period-average air quality maps.

Concentrations within the Guangzhou coupled system domains are calculated at high temporal and spatial resolution. Therefore, rather than presenting results as average concentrations over the two months as for the regional model domain, hourly concentrations are presented. For some pollutants, these detailed, hourly air quality maps relate to the metrics included in the Chinese air quality standards (specifically, the 200 µg/m³ and 160 µg/m³ standards for NO_2 and O_3 respectively, which are applicable in urban areas). Figure 5 shows a case for the Guangzhou domain where NO_2 concentrations exceed the hourly limit value in the middle of the day during May; concentrations are higher during the morning rush hour. However, Figures 5b and 5d show that the area of exceedance of the limit value of 200 µg/m³ is significantly reduced when the traffic emissions are halved; local NO_2 concentrations are not seen to change with variations in the VOC emissions (Figures 5c).

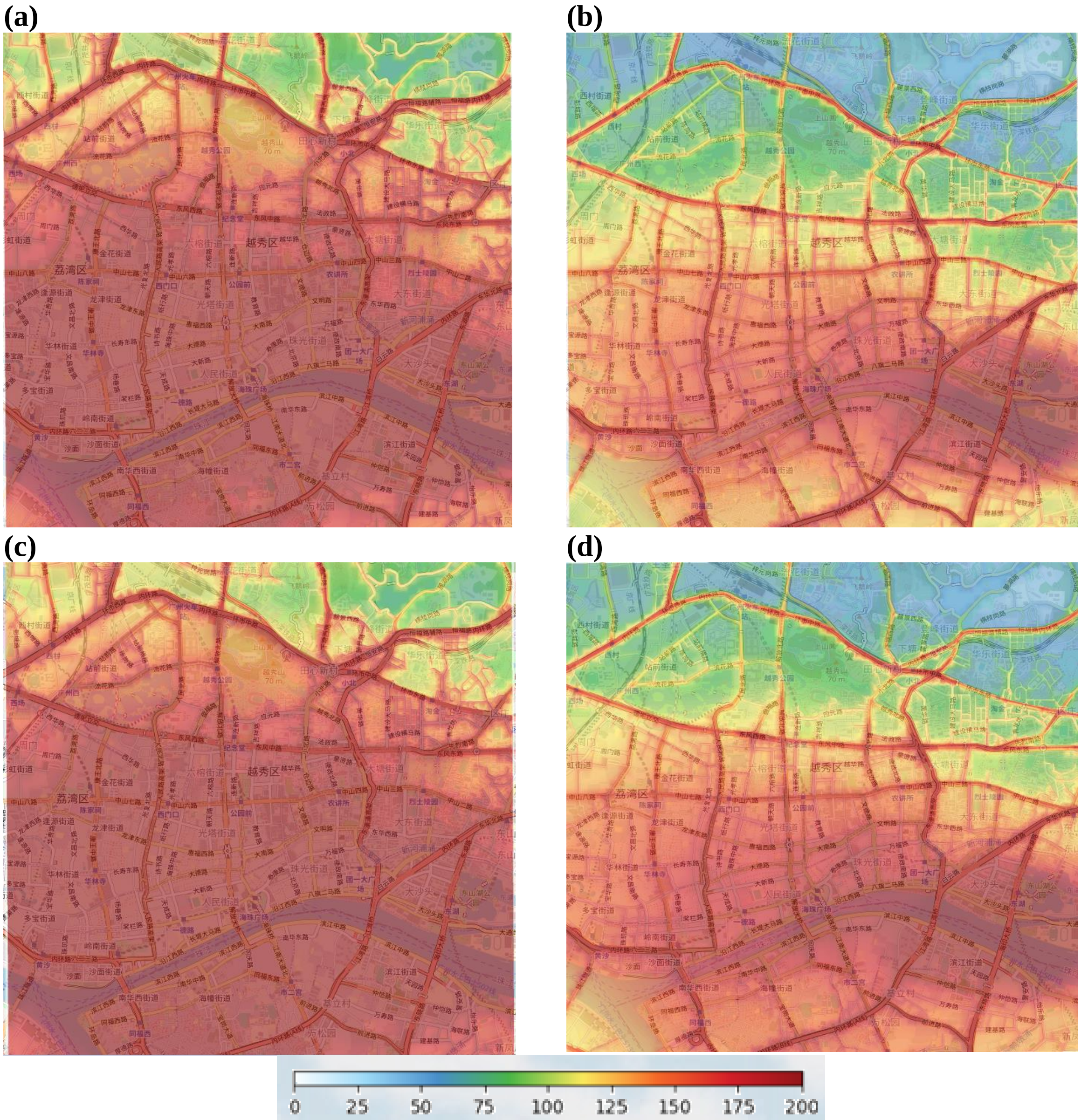

Figure 5. Simulated high-resolution spatial maps of NO_2 (Guangzhou domain) at 14:00, 10th May 2019 for a) Base case, b) Half Traffic case, c) Half Industry VOC case, d) Both Control case (µg/m^3).

Figure 6 presents O_3 concentrations in the Guangzhou domain during the same pollution episode (14:00 on 10th May 2019). As indicated earlier in relation to the regional model results, reducing traffic emissions increases the spatial extent of the O_3 exceedances in urban areas due to reduced NO_x titration of O_3 (compare Figures 6a and 6b). Conversely, reducing VOCs leads to a reduction in the area of O_3 exceedance within this local domain (compare Figures 6a and 6c). When both controls are applied in the local area (comparing Figures 6a and 6d), the net effect is a slight increase in near-road O_3 concentrations, but a decrease in concentrations elsewhere. This is an interesting result that again demonstrates the importance of accounting for both regional and local dispersion and chemistry.

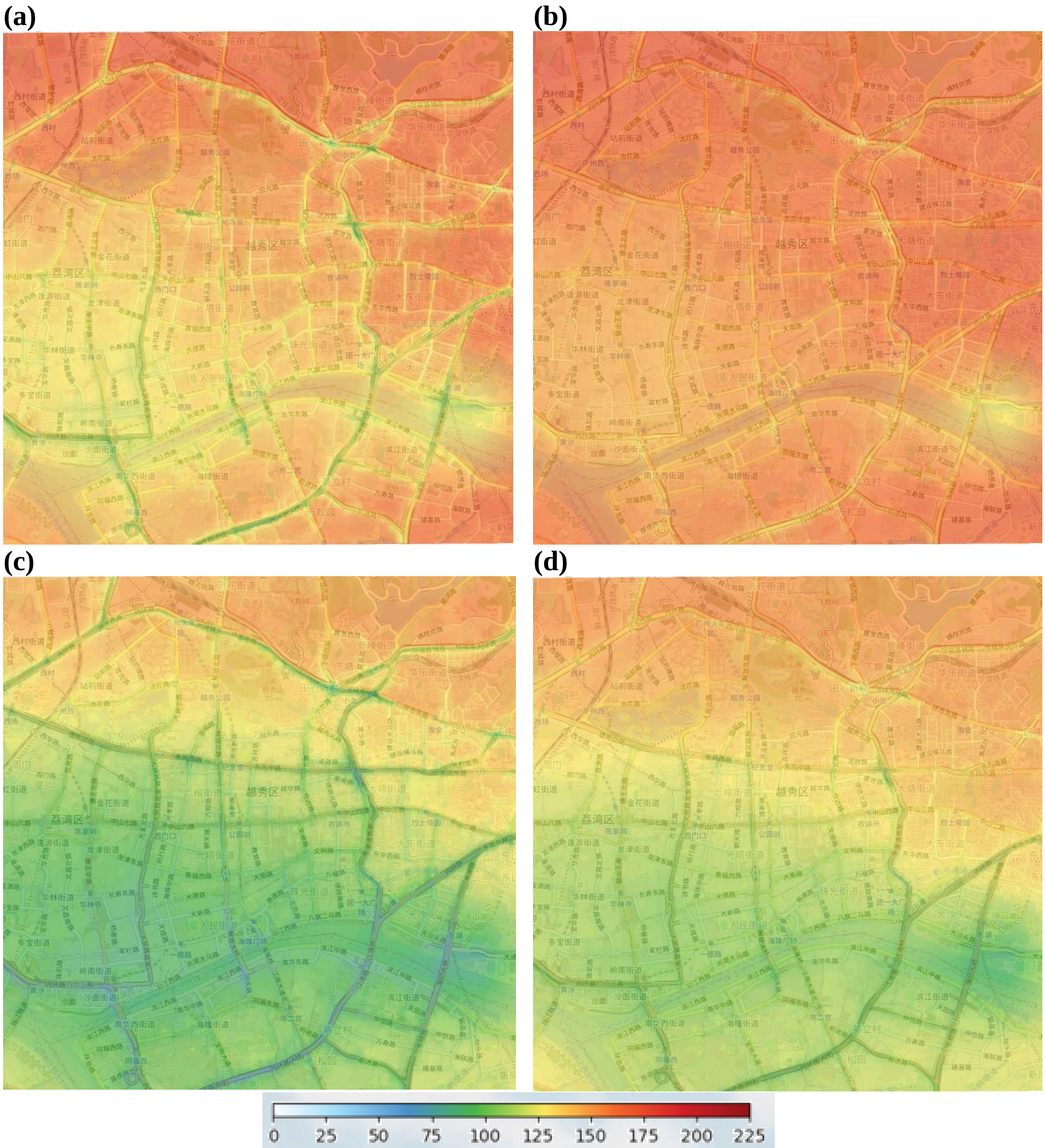

Figure 6. Simulated high-resolution spatial maps of O_3 (Guangzhou domain) at 14:00, 10th May 2019 for (a) Base case, (b) Half-Traffic case, (c) Half Industry VOC case, (d) Both-Control case ($\mu g/m^3$)

Modelled concentrations for a different time are presented for $PM_{2.5}$, as the atmospheric conditions associated with $PM_{2.5}$ pollution episodes differ from those associated with O_3 and NO_2 episodes. $PM_{2.5}$ concentrations for 11:00 on the 23rd April 2019 are shown for all four scenarios in Figure 7. Although there is a very small relative reduction in $PM_{2.5}$ emissions (Figure S2)), the impact in urban areas is significant during this episode (compare Figures 7a and 7b), as this emissions reduction relates to near-ground traffic sources. The change in VOC emissions has a negligible effect on $PM_{2.5}$ concentrations at this scale, so there is no difference between the base case and the half VOC emissions case (Figures 7a and 7c).

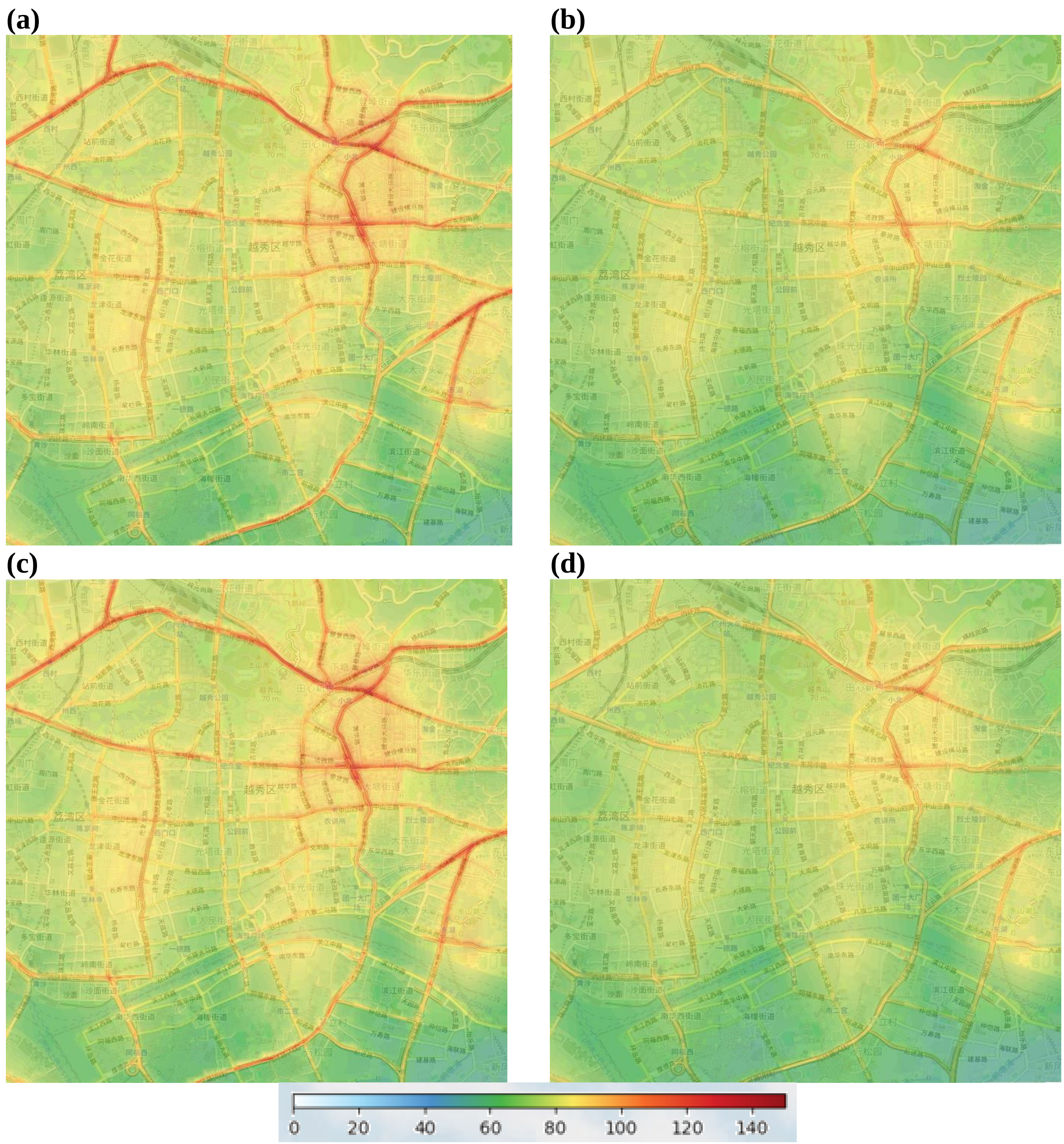

Figure 7. Simulated high-resolution spatial maps of $PM_{2.5}$ (Guangzhou domain) at 11:00, 23rd April 2019 for (a) Base case, (b) Half Traffic case, (c) Half Industry VOC case, (d) Both-Control case (µg/m^3)

3.3 Modelled concentrations at selected urban and rural locations

Pointwise concentrations are discussed in this section. Where possible, the locations considered relate to air quality measurement sites within the domain. Figure S9 shows the location of the three reference monitors located within the Guangzhou coupled system urban model domain; in addition to other pollutants, NO_2, O_3, and $PM_{2.5}$ concentrations are recorded at these sites. Figure 8 compares modelled concentrations to the measurements recorded at these three locations, for the base case and three coupled model scenarios in addition to the base case regional model. Here box plots of the short-term pollutant metrics are shown, i.e., daily maximum of the hourly NO_2, daily maximum of the 8-hour rolling O_3, and daily mean $PM_{2.5}$. As this is the first time the regional model concentrations have been presented alongside the coupled model concentrations, it is worth noting the difference in the concentrations for the two modelling approaches. Specifically, for NO_2 and $PM_{2.5}$ at the majority of sites, the coupled system predicts higher concentrations than the relatively coarse resolution regional model, and for O_3, the coupled system predicts lower concentrations. These differences are expected at the monitoring locations identified, which are strongly influenced by local road traffic source increments. The respective concentration changes of the various sensitivity scenarios in the selected monitoring stations are similar to the trend illustrated in the comparisons of the spatial concentration map. Figure 8a shows that the NO_2 concentrations are dominantly contributed from the traffic sector. The NOx titration effects on the O_3 concentration in Figure 8b drive up the O_3 concentration, while cutting the industry VOC emission sources is more effective for the O_3 control, revealing a VOC-limited regime in this region.

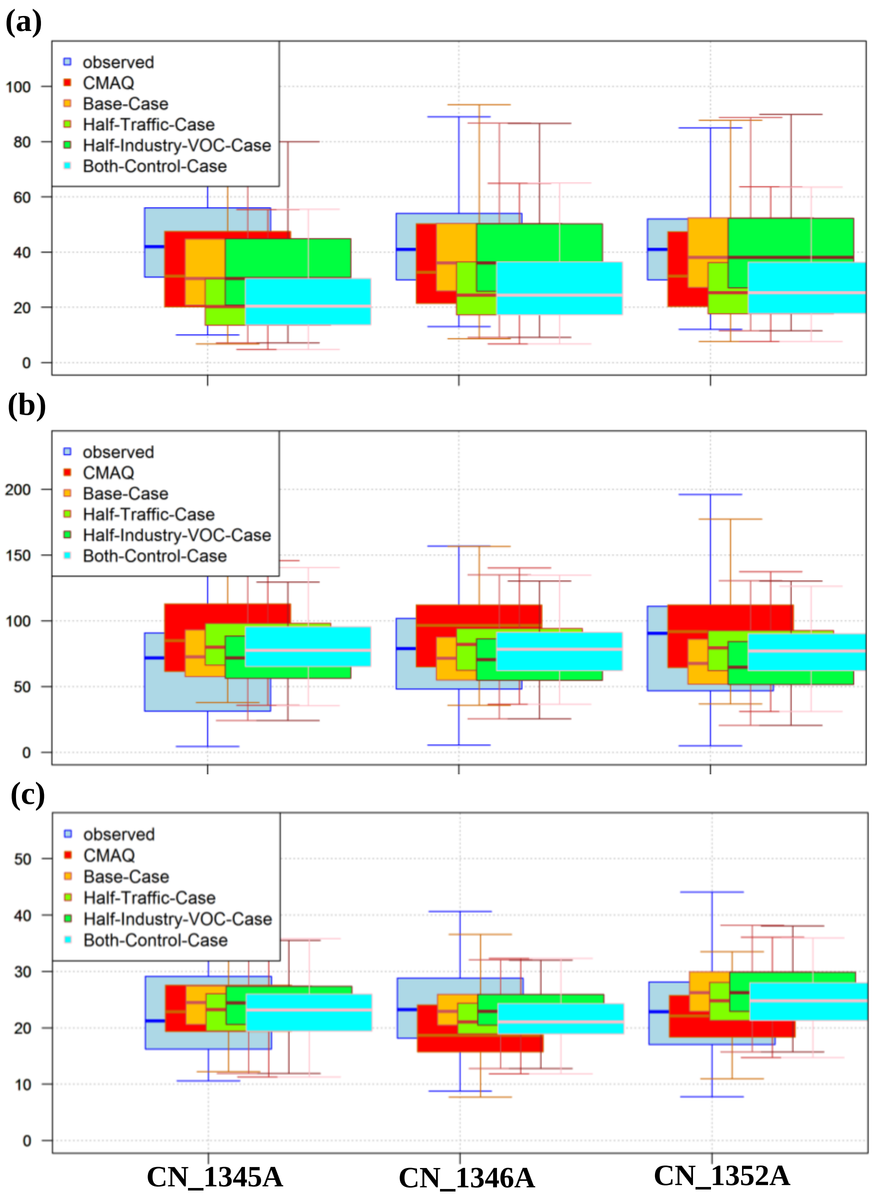

Figure 8. Box plots comparing measured concentrations (pale blue) and regional model concentrations (red) to the four high-resolution coupled system model scenarios: Base case (orange), Half Traffic case (light green), Half Industry VOC case (darker green), and both controls (bright blue) for (a) daily maximum hourly NO_2, (b) daily maximum 8-hour rolling O_3, and (c) daily average $PM_{2.5}$. Unit is in μg/m³.

In terms of the differences in modelled concentrations for the three scenarios: Over all sites, the maximum decrease in the median NO_2 hourly metric due to emission controls is over 11 µg/m³ at the roadside site CN_1352A, which corresponds to the implementation of the traffic controls. In terms of O_3, the maximum increase in the median value is over 10 µg/m³ for the reduced traffic scenario. However, this increase is reduced to under 7 µg/m³ when both controls are applied together. Decreases in median $PM_{2.5}$ are less than 2 µg/m³ for the low traffic scenario.

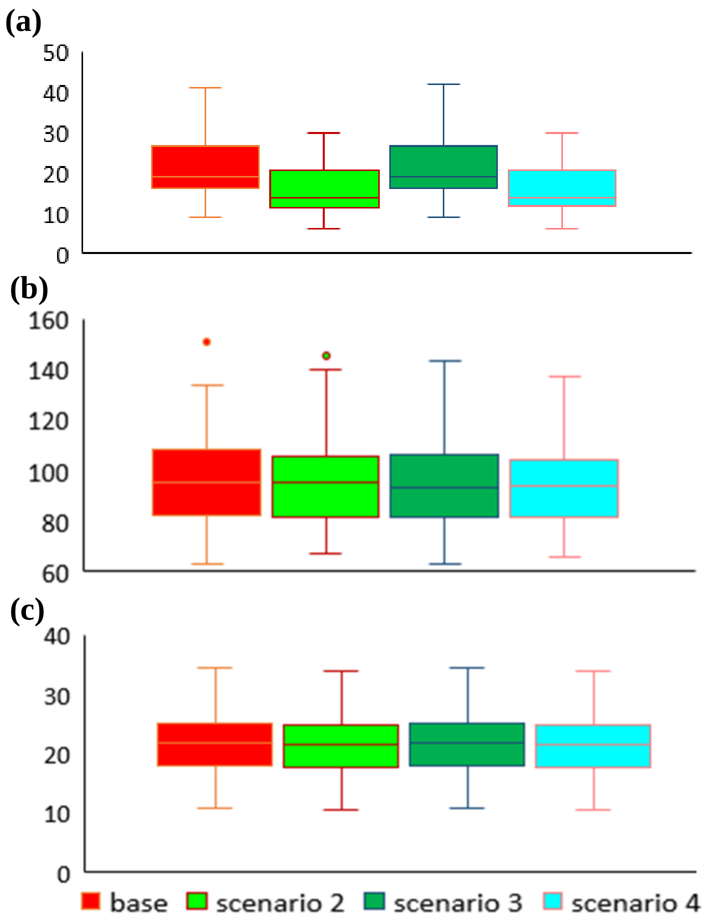

Figure 9. Box plots comparing the regional model concentrations (red) to the four high-resolution coupled system model scenarios at a rural site: Base case (red), Half Traffic case (light green), Half Industry VOC case (darker green), and both controls (bright blue) for: (a) daily maximum hourly NO_2, (b) daily maximum 8-hour rolling O_3, and (c) daily average $PM_{2.5}$. Unit is in µg/m³.

It is of interest to quantify the decrease in O_3 concentrations shown in Figures 2 and 3, to the northeast of the model domain. Unfortunately, measurements were unavailable at this rural location. Furthermore, the coupled system has only been configured for the example urban sub-domains in Guangzhou. Consequently, the only comparison to be made at this location is between concentrations calculated by the regional model. Concentration data for the location indicated by the white star in Figure 2 are presented in Figure 9; the metrics calculated for NO_2, O_3, and $PM_{2.5}$ are the same as those presented in Figure 8. At this rural location, the different emissions mitigation options only significantly alter the NO_2 concentrations, out of the three pollutants modelled. This is unsurprising because Figure S2 shows that traffic emissions make up a large proportion of NO_x emissions over the whole domain, so changes to NO_x emissions are likely to impact NO_2 concentrations in the rural as well as urban areas. Conversely, traffic makes up a relatively small proportion of primary $PM_{2.5}$ emissions; ambient $PM_{2.5}$ levels in rural areas are more influenced by industrial point and area source emissions in addition to the formation of secondary organic and inorganic particulates (Wu and Xie, 2018).

In terms of O_3, there is a relatively minimal reduction in terms of the median of maximum 8-hourly average concentrations resulting from the reduced VOC emissions scenario. This is perhaps surprising when looking back to Figure 6, as, for the corresponding scenarios, decreases of tens of µg/m³ are shown throughout the urban model domain. To understand this, it is helpful to look at a time series of modelled O_3 concentrations during an episode (Figure 10a). Here we see that while there is very little difference in concentrations for the majority of the time, the mitigation scenarios have a substantial impact in this rural location when O_3 levels are at their highest: up to 15 µg/m³ for the 8-hour rolling average metric and hourly concentration differences are greater, up to 25 µg/m³ during the same period,

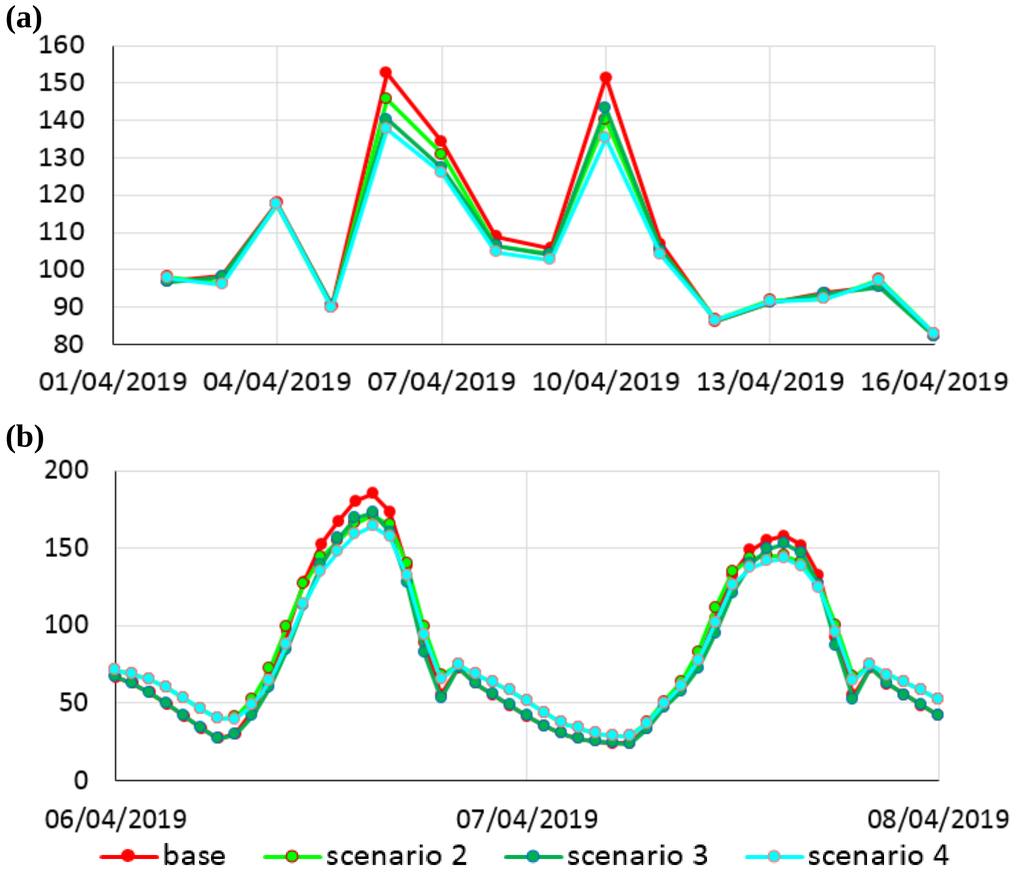

Figure 10. Regional model predictions for (a) daily-maximum 8-hourly average O_3, (b) hourly average O_3 during an episode in April 2019 at a location to the north-east of the model domain: Base case (red), Half Traffic case (light green), Half Industry VOC case (darker green), and both controls (bright blue). Unit is in µg/m^3.

4 Discussion

A regional-to-local scale coupled air quality modeling system consisting of the regional CMAQ model (Zhang et al., 2020) and the street-scale ADMS-Urban model (Biggart et al., 2020) has been configured to explore mitigation of NO_2, O_3, and $PM_{2.5}$ by controlling NO_x and VOCs in traffic and industrial sectors for the GBA, at varied resolutions. Separately, the regional and street-scale models account for pollutant dispersion and atmospheric chemistry at different temporal and spatial scales, and to varying degrees of complexity; all dominant processes are accounted for when the models are linked via the coupled system. An operational forecasting system has been developed, with street-scale resolution output at an example urban location, a 6 km x 6 km area in central Guangzhou.

Figures showing the spatial variation of emissions changes corresponding to these mitigation scenarios for NO_x, VOCs, and $PM_{2.5}$ have been presented. Graphs showing the impact of these mitigations on total emissions indicate that the combination of both controls leads to 17, 5, and 47% emissions reductions in terms of anthropogenic NO_x, $PM_{2.5}$, and VOC, respectively; of note here is that anthropogenic emissions account for a considerable part of total VOC emissions, with the remainder being from biogenic sources, which will be larger under the climate change impact (Li et al., 2018). A selection of period-average concentration plots showing the impact of the different mitigation scenarios has been presented. The regional modeling results illustrate that the half-traffic scenario leads to reductions of NO_2 and $PM_{2.5}$. Still, increases in O_3 concentrations in urban areas due to a titration effect, revealing a VOC-limited O_3 formation regime in GBA urban areas, which is consistent with previous studies (Wu et al., 2021; Zhang et al., 2021a). Conversely, this reduced traffic scenario leads to O_3 decreases in rural areas downwind. He et al. (2019) identified a VOC-limited O_3 formation regime near a rural monitoring site in GBA using a box model with the master chemistry mechanism in the Autumn of 2014. This highlights that the complex O_3 formation regime varies at different times of the year and suggests that the O_3 formation regime may transfer from VOC-limited to mixing regimes in the GBA (Wang et al., 2019a). More sensitivity analysis work needs to be done for the O_3 formation mechanism of the downwind rural areas, occurring substantial VOC emissions. The reduced industrial VOC emissions scenario leads to reduced O_3 concentrations throughout the mitigation domain but has a negligible impact on NO_2 and $PM_{2.5}$ concentrations. This sheds light on the importance of stringent VOC control measures applied to the industrial sector in the near future.

The impacts of the different mitigation options at the street scale have also been presented. For these examples, pollution maps representative of pollution levels for single hours are shown for the Guangzhou domain. These plots show the large variation in pollutant concentrations over the areas modelled: a consequence of both the regional model variations (at 1 km resolution) in addition to the local model component resolving the sharp concentration gradients in the vicinity of road sources. Similar to the regional modeling results but with more details near the roadside, the half-traffic scenario leads to large reductions of NO_2 and $PM_{2.5}$ in the vicinity of road sources; and when both controls are applied together, there is a slight increase in near-road O_3 concentrations, but a decrease in O_3 elsewhere. This highlights that synergistic controls of NO_x and VOCs would be a promising way to alleviate the $PM_{2.5}$ and O_3 simultaneously (Wu et al., 2021).

Specific locations have been selected for further analysis. Relative to the baseline, the urban air quality receptors show that the maximum decrease in the median of hourly NO_2 concentrations is over 11 µg/m³, and the maximum increase in the median of maximum 8-hour rolling O_3 concentrations is over 10 µg/m³ for the reduced traffic scenario. The O_3 increase is reduced to under 7 µg/m³ when both controls are considered, indicating the effectiveness of the synergistic control measures of NO_x and VOC in both sectors. The decreases in the daily average $PM_{2.5}$ metrics are less than 2 µg/m³ for the reduced traffic scenario, confirming that the $PM_{2.5}$ primary emissions from traffic sources have a relatively low contribution to overall concentrations (Figure S2). The magnitude of these relative changes should be taken in the context of the metric considered: hourly values (i.e., NO_2) demonstrate the greatest variations because the maximum differences at peak traffic times are quantified; conversely, for daily average values (i.e., for $PM_{2.5}$), the impact of peak values is smoothed out by the inclusion of hours where pollutant concentrations may be dominated by regional rather than local air pollution. O_3 episodes are of particular current interest to government officials and stakeholders. The modelling work has demonstrated that whilst O_3 concentrations increase in the urban areas as a result of the mitigation options considered, O_3 decreases downwind. Inspection of modelled pollutant concentrations at a rural location to the northeast of the modelling domain during an O_3 episode shows that concentrations are reduced by up to 15 μg/m³ for the 8-hour metric and up to 25 μg/m³ for the 1-hour metric, which emphasizes the value of more stringent VOC controls, applied to the industrial sector.

5 Conclusion

To address the challenges of controlling $PM_{2.5}$ and O_3 concentrations simultaneously using an ultrahigh spatial resolution approach, this study presents the regional air quality model CMAQ coupled to the street-scale model ADMS-Urban. The coupled system allows a thorough assessment of the impact that NO_x and VOC emissions from traffic and industry have on ambient O_3 and $PM_{2.5}$, drawing a holistic pollution mitigation picture at a range of spatial resolutions, as well as highlighting the temporal relationship between emissions, meteorological conditions and O_3 concentrations. The regional modeling results show the half-traffic scenario leads to reductions of NO_2 and $PM_{2.5}$, but increases in O_3 concentrations in urban areas (and decreases in rural areas downwind), revealing a VOC-limited O_3 formation regime. The reduced industrial VOC emissions scenario leads to reduced O_3 concentrations throughout the mitigation domain; it has a negligible impact on NO_2 and $PM_{2.5}$ concentrations. This finding suggests more stringent VOC control measures in the industrial sector will substantially alleviate the increasing O_3 pollution.

With coupling, the street-scale ADMS-Urban model resolves the sharp concentration gradients in the vicinity of road sources, and the half-traffic scenario leads to large reductions of NO_2 and $PM_{2.5}$ in those locations. When both controls are applied together, there is a slight increase in near-road O_3 concentrations, but a decrease in O_3 elsewhere. Examples of urban and rural monitoring sites in central Guangzhou are used to better interpret findings. Relative to the base case, the maximum decrease in the median hourly NO_2 metric is over 11 μg/m³ for the reduced traffic scenario; the maximum increase in the median maximum 8-hour rolling O_3 metric is over 10 μg/m³ for the reduced traffic scenario, although this increase is reduced to under 7 μg/m³ when both controls are considered; and decreases in the daily average $PM_{2.5}$ metrics are less than 2 μg/m³ for the reduced traffic scenario.

Although the detailed mitigation pathways modeled here support the second phase of the Air Pollution Prevention and Control Action Plan—the Three-Year Action Plan for Clean Air—released by the State Council of China in 2018, further refinements are required as part of future studies. Subsequent studies would benefit from: analysis using a more comprehensive observational pollutant concentrations dataset; application of the model over larger urban areas in the region; and application of the coupled street-scale air quality modeling system to similar urban cities. In addition, a more advanced emission preparation methodology (Lam et al., 2021) must be applied in order to minimize the uncertainties associated with the emission inventory, and more elaborate emission sources could be modelled explicitly in the ADMS-Urban model, e.g., industrial stacks (Hood et al., 2018). Since the meteorological fields such as the wind are of great importance to the coupled model simulations (Wang et al., 2019b), improving the representation of urban morphological data in the model could improve the baseline model biases. Finally, assessing the reduction radios of NO_x and VOC in various areas of a city or different cities should be cautiously assessed for efficient complex co-photochemical controls.

Acknowledgements

We sincerely thank the Hong Kong Environmental Protection Department (EPD) for providing the bottom-up emission inventory. We appreciate the Guangdong Environmental Monitoring Centre, Macao EPD, and HK EPD for offering the observational data to validate the model runs. All of the data used in this paper are cited and referred to in the reference list. The authors would like to acknowledge funding from the Newton Fund through Innovate UK as part of the project titled Air Pollution Monitoring and Very High Resolution Early Warning Platform for Guangdong (project number 104313), Science and Technology Planning Project of Guangdong Province (2018A050501004), and HSBC 150th Anniversary Charity Programme through the PRAISE-HK project.

References

Biggart, M., Stocker, J., Doherty, R.M., Wild, O., Hollaway, M., Carruthers, D., Li, J., Zhang, Q., Wu, R., Kotthaus, S., 2020. Street-scale air quality modelling for Beijing during a winter 2016 measurement campaign. Atmospheric Chemistry and Physics 20, 2755-2780.

Cai, S., Ma, Q., Wang, S., Zhao, B., Brauer, M., Cohen, A., Martin, R.V., Zhang, Q., Li, Q., Wang, Y., 2018. Impact of air pollution control policies on future $PM_{2.5}$ concentrations and their source contributions in China. Journal of Environmental Management 227, 124-133.

Carruthers, D., Holroyd, R., Hunt, J., Weng, W., Robins, A., Apsley, D., Thompson, D., Smith, F., 1994. UK-ADMS: A new approach to modelling dispersion in the earth's atmospheric boundary layer. Journal of Wind Engineering and Industrial Aerodynamics 52, 139-153.

Che, W., Frey, H.C., Fung, J.C., Ning, Z., Qu, H., Lo, H.K., Chen, L., Wong, T.-W., Wong, M.K., Lee, O.C., 2020. PRAISE-HK: A personalized real-time air quality informatics system for citizen participation in exposure and health risk management. Sustainable Cities and Society 54, 101986.

Cheng, J., Tong, D., Zhang, Q., Liu, Y., Lei, Y., Yan, G., Yan, L., Yu, S., Cui, R.Y., Clarke, L., 2021. Pathways of China's $PM_{2.5}$ air quality 2015–2060 in the context of carbon neutrality. National Science Review.

Conibear, L., Reddington, C.L., Silver, B.J., Knote, C., Arnold, S.R., Spracklen, D.V., 2021. Regional policies targeting residential solid fuel and agricultural emissions can improve air quality and public health in the Greater Bay Area and across China. GeoHealth, e2020GH000341.

Cui, R.Y., Hultman, N., Cui, D., McJeon, H., Yu, S., Edwards, M.R., Sen, A., Song, K., Bowman, C., Clarke, L., 2021. A plant-by-plant strategy for high-ambition coal power phaseout in China. Nature Communications 12, 1-10.

Gong, K., Li, L., Li, J., Qin, M., Wang, X., Ying, Q., Liao, H., Guo, S., Hu, M., Zhang, Y., 2021. Quantifying the impacts of inter-city transport on air quality in the Yangtze River Delta urban agglomeration, China: Implications for regional cooperative controls of $PM_{2.5}$ and O_3. Science of the Total Environment 779, 146619.

He, Z., Wang, X., Ling, Z., Zhao, J., Guo, H., Shao, M., Wang, Z., 2019. Contributions of different anthropogenic volatile organic compound sources to ozone formation at a receptor site in the Pearl River Delta region and its policy implications. Atmospheric Chemistry and Physics 19, 8801-8816.

Hood, C., MacKenzie, I., Stocker, J., Johnson, K., Carruthers, D., Vieno, M., Doherty, R., 2018. Air quality simulations for London using a coupled regional-to-local modelling system. Atmospheric Chemistry and Physics 18, 11221-11245.

Hood, C., Stocker, J., Seaton, M., Johnson, K., O'Neill, J., Thorne, L., Carruthers, D., 2021. Comprehensive evaluation of an advanced street canyon air pollution model. Journal of the Air & Waste Management Association 71, 247-267.

Jiang, X., Hong, C., Zheng, Y., Zheng, B., Guan, D., Gouldson, A., Zhang, Q., He, K., 2015. To what extent can China's near-term air pollution control policy protect air quality and human health? A case study of the Pearl River Delta region. Environmental Research Letters 10, 104006.

Jiang, X., Yoo, E.-h., 2018. The importance of spatial resolutions of community multiscale air quality (CMAQ) models on health impact assessment. Science of the Total Environment 627, 1528-1543.

Lam, Y., Fu, J., 2010. A novel downscaling technique for the linkage of global and regional air quality modeling. Atmospheric Chemistry and Physics, 4013.

Lam, Y.F., Cheung, C.C., Zhang, X., Fu, J.S., Fung, J.C.H., 2021. Development of New Emission Reallocation Method for Industrial Nonpoint Source in China. Atmospheric Chemistry and Physics, https://doi.org/10.5194/acp-2020-1330.

Lao, J., Teixidó, O., 2011. Air quality model for Barcelona. Air Pollution 19, 25-36.

Li, K., Jacob, D.J., Liao, H., Shen, L., Zhang, Q., Bates, K.H., 2019a. Anthropogenic drivers of 2013–2017 trends in summer surface ozone in China. Proceedings of the National Academy of Sciences 116, 422-427.

Li, K., Jacob, D.J., Liao, H., Zhu, J., Shah, V., Shen, L., Bates, K.H., Zhang, Q., Zhai, S., 2019b. A two-pollutant strategy for improving ozone and particulate air quality in China. Nature Geoscience 12, 906-910.

Li, L., Hu, J., Li, J., Gong, K., Wang, X., Ying, Q., Qin, M., Liao, H., Guo, S., Hu, M., 2021a. Modelling air quality during the EXPLORE-YRD campaign–Part II. Regional source apportionment of ozone and $PM_{2.5}$. Atmospheric Environment 247, 118063.

Li, M., Zhang, D., Li, C.-T., Selin, N.E., Karplus, V.J., 2019c. Co-benefits of China's climate policy for air quality and human health in China and transboundary regions in 2030. Environmental Research Letters 14, 084006.

Li, N., He, Q., Greenberg, J., Guenther, A., Li, J., Cao, J., Wang, J., Liao, H., Wang, Q., Zhang, Q., 2018. Impacts of biogenic and anthropogenic emissions on summertime ozone formation in the Guanzhong Basin, China. Atmospheric Chemistry and Physics 18, 7489-7507.

Li, Y., Xu, H., Tang, K., Lau, A., Fung, J., Zhang, X., 2021b. An Ensemble Assessment of the Effectiveness of Vehicular Emission Control Programs for Air Quality Improvement in Hong Kong. Atmospheric Environment, 118571.

Liu, T., Wang, C., Wang, Y., Huang, L., Li, J., Xie, F., Zhang, J., Hu, J., 2020. Impacts of model resolution on predictions of air quality and associated health exposure in Nanjing, China. Chemosphere 249, 126515.

Qin, Y., Wagner, F., Scovronick, N., Peng, W., Yang, J., Zhu, T., Smith, K.R., Mauzerall, D.L., 2017. Air quality, health, and climate implications of China's synthetic natural gas development. Proceedings of the National Academy of Sciences 114, 4887-4892.

Silveira, C., Ferreira, J., Miranda, A.I., 2019. The challenges of air quality modelling when crossing multiple spatial scales. Air Quality, Atmosphere & Health 12, 1003-1017.

Silver, B., Conibear, L., Reddington, C.L., Knote, C., Arnold, S.R., Spracklen, D.V., 2020. Pollutant emission reductions deliver decreased $PM_{2.5}$-caused mortality across China during 2015–2017. Atmospheric Chemistry and Physics 20, 11683-11695.

Stocker, J., Hood, C., Carruthers, D., McHugh, C., 2012. ADMS-Urban: developments in modelling dispersion from the city scale to the local scale. International Journal of Environment and Pollution 50, 308-316.

Tao, H., Xing, J., Zhou, H., Pleim, J., Ran, L., Chang, X., Wang, S., Chen, F., Zheng, H., Li, J., 2020. Impacts of improved modeling resolution on the simulation of meteorology, air quality, and human exposure to $PM_{2.5}$, O_3 in Beijing, China. Journal of Cleaner Production 243, 118574.

Tong, D., Cheng, J., Liu, Y., Yu, S., Yan, L., Hong, C., Qin, Y., Zhao, H., Zheng, Y., Geng, G., 2020. Dynamic projection of anthropogenic emissions in China: methodology and 2015–2050 emission pathways under a range of socio-economic, climate policy, and pollution control scenarios. Atmospheric Chemistry and Physics 20, 5729-5757.

Wang, N., Lyu, X., Deng, X., Huang, X., Jiang, F., Ding, A., 2019a. Aggravating O_3 pollution due to NO_x emission control in eastern China. Science of the Total Environment 677, 732-744.

Wang, P., Guo, H., Hu, J., Kota, S.H., Ying, Q., Zhang, H., 2019b. Responses of $PM_{2.5}$ and O_3 concentrations to changes of meteorology and emissions in China. Science of the Total Environment 662, 297-306.

Wang, X., Li, L., Gong, K., Mao, J., Hu, J., Li, J., Liu, Z., Liao, H., Qiu, W., Yu, Y., 2021. Modelling air quality during the EXPLORE-YRD campaign–Part I. Model performance evaluation and impacts of meteorological inputs and grid resolutions. Atmospheric Environment 246, 118131.

Wu, J., Wang, Y., Liang, J., Yao, F., 2021. Exploring common factors influencing $PM_{2.5}$ and O_3 concentrations in the Pearl River Delta: Tradeoffs and synergies. Environmental Pollution, 117138.

Wu, R., Liu, F., Tong, D., Zheng, Y., Lei, Y., Hong, C., Li, M., Liu, J., Zheng, B., Bo, Y., 2019. Air quality and health benefits of China's emission control policies on coal-fired power plants during 2005–2020. Environmental Research Letters 14, 094016.

Wu, R., Xie, S., 2018. Spatial distribution of secondary organic aerosol formation potential in China derived from speciated anthropogenic volatile organic compound emissions. Environmental science & technology 52, 8146-8156.

Yli-Pelkonen, V., Scott, A.A., Viippola, V., Setälä, H., 2017. Trees in urban parks and forests reduce O_3, but not NO_2 concentrations in Baltimore, MD, USA. Atmospheric Environment 167, 73-80.

Zhang, C., Chen, M., Li, R., Ding, Y., Lin, H., 2015. A virtual geographic environment system for multiscale air quality analysis and decision making: A case study of SO_2 concentration simulation. Applied Geography 63, 326-336.

Zhang, X., Fung, J.C., Lau, A.K., Hossain, M.S., Louie, P.K., Huang, W., 2021a. Air quality and synergistic health effects of ozone and nitrogen oxides in response to China's integrated air quality control policies during 2015–2019. Chemosphere 268, 129385.

Zhang, X., Fung, J.C., Lau, A.K., Zhang, S., Huang, W., 2021b. Improved Modeling of Spatiotemporal Variations of Fine Particulate Matter Using a Three-Dimensional Variational Data Fusion Method. Journal of Geophysical Research: Atmospheres 126, e2020JD033599.

Zhang, X., Fung, J.C., Zhang, Y., Lau, A.K., Leung, K.K., Huang, W.W., 2020. Assessing $PM_{2.5}$ emissions in 2020: The impacts of integrated emission control policies in China. Environmental Pollution 263, 114575.

Zhao, H., Chen, K., Liu, Z., Zhang, Y., Shao, T., Zhang, H., 2021. Coordinated control of $PM_{2.5}$ and O_3 is urgently needed in China after implementation of the "Air pollution prevention and control action plan". Chemosphere 270, 129441.